Theory of polarization-controlled polariton logic gates

T. Ostatnický,[1,2] I. A. Shelykh,[3] and A. V. Kavokin[1,4]
[1]*School of Physics and Astronomy, University of Southampton, Highfield, Southampton SO17 1BJ, United Kingdom*
[2]*Faculty of Mathematics and Physics, Charles University, Ke Karlovu 3, 121 16 Praha 2, Czech Republic*
[3]*Science Institute, University of Iceland, Dunhagi 3, IS-107 Reykjavik, Iceland*
[4]*Faculta di Fisica, Universita di Roma II "Tor Vergata," 1 via della Ricerca Scientifica, 00173 Roma, Italy*
(Received 3 September 2009; revised manuscript received 23 February 2010; published 15 March 2010)

Elastic scattering of exciton polaritons in planar semiconductor microcavities has been used to create X-NOR logic gates. Polaritons with identical linear polarization scatter preferentially at the right angle and rotate their polarization by 90°. On the other hand, scattering of polaritons having orthogonal linear polarizations is suppressed. We show that these effects are a consequence of the multiple scattering in microcavities which involve three and more polaritons. The theory quantitatively reproduces the experimental data of C. Leyder *et al.* [Phys. Rev. Lett. **99**, 196402 (2007)].

DOI: 10.1103/PhysRevB.81.125319 PACS number(s): 71.36.+c, 42.65.Yj, 72.25.Rb

I. INTRODUCTION

Exciton polaritons, also referred to as cavity polaritons, are elementary excitations in semiconductor microcavities.[1] Being a combination of bosonic crystal excitations [quantum well (QW) excitons] and photons, cavity polaritons posses a number of peculiar properties, which make them promising candidates for observation of interesting collective phenomena, including high-T_c Bose-Einstein condensation (BEC) (Ref. 2) and superfluidity.[3]

An important peculiarity of a polariton system is the spin structure of a polariton state: being formed usually by heavy-hole excitons, polaritons have two allowed spin projections on the structure growth axis (± 1), corresponding to the right and left circular polarizations of counterpart photons. The exciton states having spin projections ± 2 (dark states) are split-off in energy and affect the polariton dynamics in the second order with respect to perturbation caused by Coulomb interaction between the exciton polaritons.[4] The polarization of light emitted by a microcavity is the same as the polarization of exciton polaritons. From the formal point of view the spin structure of cavity polaritons is analogous to spin structure of the electrons (both are two-level systems), which is why a concept of a pseudospin vector $\mathbf{S}$ is suitable for the description of their polarization.[5] The pseudospin is a quantum analogy of the Stockes vector of a classical light. It is linked with a 2×2 spin-density matrix ρ of a polariton quantum state by a relation,

$$\rho = \frac{N}{2}\mathbf{I} + \mathbf{S}\cdot\sigma, \tag{1}$$

where N is the occupation number of the polariton state, $\mathbf{I}$ is the identity matrix, and σ is the Pauli-matrix vector. The orientation of the pseudospin determines the polarization of emission from a microcavity. The parameter $\rho = 2|\mathbf{S}|/N$ is the total polarization degree of light emitted by the cavity, which may vary between 0 and 1. The z component of the pseudospin is linked with the circular polarization degree of emitted light $\rho_c = 2S_z/N$, while S_x and S_y characterize the linear polarization degree of emitted light measured in (x,y) axes (ρ_l) and in the diagonal axes (ρ_d), respectively: $\rho_l \equiv 2S_x/N$, $\rho_d \equiv 2S_y/N$.

In the absence of an external magnetic field the "spin-up" and "spin-down" states of the exciton polaritons corresponding to their spin projections $+1$ and -1 to z axis and the pseudospin parallel and antiparallel to z axis, respectively, are degenerate. On the other hand, the interaction of polaritons in triplet configuration (identical spin projections on the structure growth axis) is usually much stronger than that of polaritons in singlet configuration[6–8] (spin projections of different signs). This may lead to lifting of degeneracy of the spin-up and spin-down polariton states if their populations are not equal. The spin state which is stronger populated has a higher energy than the spin state which is less populated. This interaction-induced spin splitting may be described as an effective magnetic field applied in z direction which causes the Larmor precession of the polariton pseudospin in the (x,y) plane.[9] This precession, also referred to as the self-induced Larmor precession, is responsible for the mixing of linearly polarized polariton states which manifests itself in remarkable nonlinear effects in polariton spin relaxation.[8] The difference in the polariton-polariton interaction constants in singlet and triplet configurations is also responsible for the predominantly linear polarization of BECs of exciton polaritons, recently observed in microcavities at the conditions close to the thermal equilibirum.[10]

From the point of view of potential applications, it has been recently pointed out that the controllable manipulation of the pseudospin of cavity polaritons can provide a basis for the construction of optoelectronic devices of the new generation, referred to as spin-optronic devices,[11] which can be of importance in various technological implementations including the classical or quantum information transfer. With respect to the conventional spintronics operating with electrically charged spin carriers, the spin optronics has an advantage of strongly reducing the dramatic impact of carrier spin relaxation or decoherence,[12] which severely limits the functionality of spintronic devices. Macroscopically large coherence lengths of exciton polaritons and their bosonic properties led to formulation of several concepts of spin-optronic devices based on microcavities. These include in particular mesoscopic optical interferometers,[13] optical

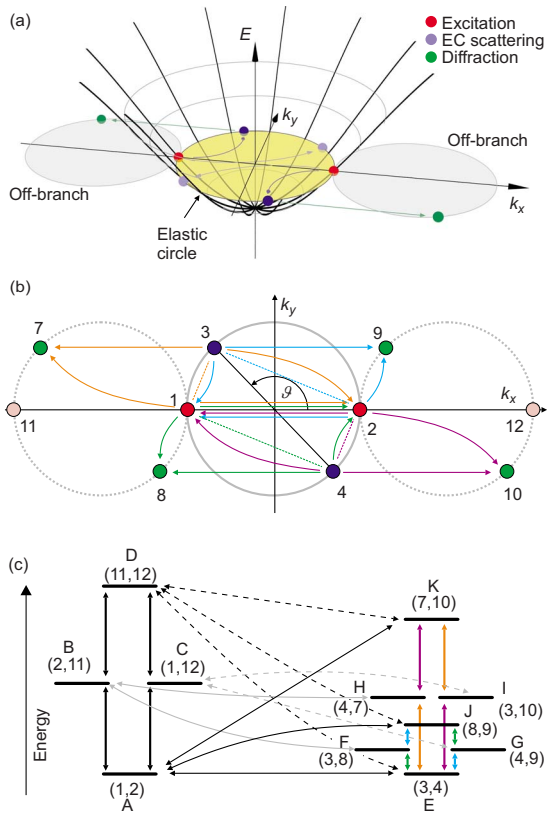

FIG. 1. (Color online) (a) Scheme of the polariton dispersion in the two-dimensional reciprocal space and scattering of counterpropagating polaritons (denoted as "Excitation") forming scattered pairs on the elastic circle ("EC scattering") and their further diffraction to off-branches ("Diffraction"). (b) Diffraction of the EC scattered state to the off-branch states (lying on the dashed circles). Lines denote the pair of interacting polaritons and arrows with the appropriate color denote the possible diffraction processes. (c) Level scheme for visualization of the virtual processes. Numbers refer to the states in (b).

circuits,[14] and highly efficient sources of entangled photon pairs.[15]

The polarization-controlled X-NOR gate is the only spin-optronic device concept which has been realized experimentally already.[16] It consists of a semiconductor microcavity in the strong-coupling regime optically excited by two linearly polarized light beams incident at the opposite oblique angles [see Fig. 1(a)]. The device operates due to elastic polariton-polariton scattering which changes distribution of the exciton polaritons on the so-called elastic circle, i.e., the circle in the reciprocal space corresponding to the constant energy, equal to the energy of the pump beams. It has been demonstrated experimentally that polaritons are scattered preferentially at the right angle in this configuration (i.e., in the directions which are characterized by in-plane wave vector components orthogonal to those of the pump beams[17]). Moreover, the scattering only takes place if two pumping light beams are colinearly polarized. On the other hand, if the polarizations of two incident beams are orthogonal, the scattering vanishes. This surprising experimental observation has been theoretically reproduced in Ref. 16 using the spin dependent Gross-Pitaevskii (GP) equations, which describe the ensemble of exciton polaritons by a single spinor wave function. Being a powerful tool for numerical modeling of the coherent polariton dynamics, GP equations account for polariton-polariton scattering in all orders assuming contact interactions described by two phenomenological constants α_1 and α_2 which characterize the scattering of polaritons with parallel and antiparallel spins, respectively. GP equations do not provide information on the probabilities and polarization selection rules of each individual scattering act and, while the agreement between simulation and experiment is excellent, the physical reasons of the unusual characteristics of the polariton X-NOR gates remained obscure.

The goal of this paper is to describe the most important features of polariton logic gates in terms of the spin- and angle-dependent scattering of exciton polaritons. We show that the peculiar nonuniform distribution of the polaritons on the elastic circle observed in Refs. 16 and 17 is due to the diffraction of scattered polaritons on the grating created by two pump pulses.

II. POLARITON X-NOR GATE IN THE SPONTANEOUS SCATTERING REGIME

Polarization selection rules in the course of polariton-polariton scattering have been analyzed in our recent publication.[18] We have shown that a single spontaneous scattering act of two identically linearly polarized exciton polaritons results in two weakly polarized polariton states having their preferential polarization in the plane orthogonal to the polarization plane of two initial states. This small preferential polarization of the final states may be amplified in the case of stimulated scattering. On the other hand, no significant angular dependence of the scattering amplitudes has been found for the realistic microcavity structures within this model. This result is in apparent contradiction with the experiments[17] and the Gross-Pitaevskii model.[16] Having in mind that the GP equations implicitly account for polariton-polariton scattering in all orders, the only possible explanation of this contradiction is that the experimentally observed strong angular dependence of the scattered polariton population is due to the processes involving two or more polariton scattering events.

To start we note that there is no process which could break the cylindrical symmetry of the microcavity potential acting upon exciton polaritons under weak excitation (i.e., if pump-induced blueshift of the excited states is small compared to the disorder potential in the sample); however, when the pump power is sufficiently large, the pump beams themselves provide the symmetry-breaking effect. This effect can be described as an appearance of a pump-induced transient grating on which the polaritons diffract from the elastic circle (EC) to off-branches[19] shifted in the reciprocal space by the grating vector $\pm(\boldsymbol{k}_1-\boldsymbol{k}_2)$, where $\boldsymbol{k}_{1,2}$ are the in-plane wave vectors of excitation beams [see Fig. 1(a)]. The transitions to the off-branches do not conserve energy so that they must be accompanied by processes which restore the energy conservation within time inversely proportional to the energy mismatch, according to the uncertainty relations. There is a rich variety of processes which may restore the energy con-

servation, including scattering back to elastic circle, phonon scattering, polariton decay by tunneling of a photon through Bragg mirrors (photon would have energy of a polariton on the EC and wave vector of the off-branch state), or return of polaritons to their initial states. The retarded return processes influence the phase of the involved polariton so that the interference of polaritons coming back from the virtual states with other polaritons is not necessarily constructive. In this paper, we show that the diffraction of the virtual states is responsible for modulation of the polariton population on the elastic circle even though this effect is weak compared to the direct scattering from the pump states to the states on the elastic circle.

We distinguish between *EC scattering* and *diffraction* throughout the paper. We define *EC scattering* as a wave vector conserving elastic-scattering process for a pair of polaritons. In particular, the resonant scattering of pump polaritons to the states at the elastic circle is EC scattering. The diffraction is scattering of a single exciton polariton on a diffraction grating formed by two pump beams which leads to the change of the polariton wave vector by $\pm(\boldsymbol{k}_1-\boldsymbol{k}_2)$. When we refer to both processes together, we shall use the term *scattering*.

The system reveals a rich variety of possible pair interactions which populate real or virtual states and contribute to the overall dynamics. There are, nevertheless, several processes in the limit of weak polariton-polariton interactions, which are more probable than others: these are (1) resonant processes (scattering around the EC) and (2) virtual processes, enhanced by the large conjoint population of the involved states. The strongest transitions from one to the other pump beam are stimulated due to their large macroscopic populations. The exchanged wave vector is $\pm(\boldsymbol{k}_1-\boldsymbol{k}_2)$ in this case and therefore this group of processes represents the diffraction.

In order to describe the system dynamics in the spontaneous EC scattering regime (i.e., considering low population of the EC), we consider a polariton pair and investigate its evolution, accounting for the background populations $n_{1,2}$ of the pump beams. Considering only those single-polariton states which may be populated by a single EC scattering or diffraction,[20] single polaritons may occupy only states 1–12 depicted in Fig. 1(b). All the two-polariton states allowed by the dynamics may be denoted as follows: the initial state is $A=(1,2)$, where the numbers in parentheses denote the contributing single-polariton states, the final EC scattered state (for a fixed scattering angle ϑ) is $E=(3,4)$. These states on the EC are coupled to the virtual states $B-D,F-K$ by diffraction, see description of levels in Fig. 1(c). The states D, J and K are virtual off-branch states. Their relative influence on the scattering of polaritons depends on the scattering angle. The state D and, in many cases, one of the states J and K or sometimes even both of them can be neglected as they have a little influence on the population of the elastic circle. On the other hand, for specific scattering angles one of the states J or K may lie close to the EC and play a more important role in its population, consequently. In the numerical calculation we always keep the states D, J, and K in consideration. According to the Fig. 1(c), diffraction of e.g., single-polariton state 3 may be regarded as scattering of the states $1,3\rightarrow 2,7$ or $2,3\rightarrow 1,9$ and therefore it leads to efficient coupling of the state E to G and H. Note, however, that there is no state (1,1) in the level scheme. To clarify this point, we need to consider both the polariton pair and the background population—wave vector conservation requires that the transition $(1,2)\rightarrow(1,1)$ is accompanied by the increase of the population of state 2 by 1 polariton, making the initial and the final-state equivalent. Clearly the states $A-D$ form a group coupled by diffraction and also all states within the second group $E-K$ are coupled by diffraction. These two groups are then coupled by EC scattering as depicted in Fig. 1(c). The relevant effective Hamiltonian for the first group $(A-D)$ accounting only for diffraction reads as

$$H_{A-D}=\begin{pmatrix} 0 & V_{\mathrm{D}} & V_{\mathrm{D}} & 0 \\ V_{\mathrm{D}} & \hbar\omega_{11} & 0 & V_{\mathrm{D}} \\ V_{\mathrm{D}} & 0 & \hbar\omega_{11} & V_{\mathrm{D}} \\ 0 & V_{\mathrm{D}} & V_{\mathrm{D}} & 2\hbar\omega_{11} \end{pmatrix}, \tag{2}$$

where we denote $\hbar\omega_{11}$ the energy mismatch between the single-polariton state 11 and the EC which can be evaluated as $\hbar\omega_{11}=4\hbar^2k_0^2/m^*$ in parabolic approximation, where k_0 is the EC radius and m^* is the polariton effective mass (in the presence of strong excitation field, parabolic approximation may be altered by a more proper dispersion accounting for the Bogoliubov renormalization[19,21]). The effective Hamiltonian for the group $(E-K)$ has the following form:

$$H_{E-K}=\begin{pmatrix} 0 & V_{\mathrm{D}} & V_{\mathrm{D}} & V_{\mathrm{D}} & V_{\mathrm{D}} & 0 & 0 \\ V_{\mathrm{D}} & \hbar\omega_8 & 0 & 0 & 0 & V_{\mathrm{D}} & 0 \\ V_{\mathrm{D}} & 0 & \hbar\omega_8 & 0 & 0 & V_{\mathrm{D}} & 0 \\ V_{\mathrm{D}} & 0 & 0 & \hbar\omega_7 & 0 & 0 & V_{\mathrm{D}} \\ V_{\mathrm{D}} & 0 & 0 & 0 & \hbar\omega_7 & 0 & V_{\mathrm{D}} \\ 0 & V_{\mathrm{D}} & V_{\mathrm{D}} & 0 & 0 & 2\hbar\omega_8 & 0 \\ 0 & 0 & 0 & V_{\mathrm{D}} & V_{\mathrm{D}} & 0 & 2\hbar\omega_7 \end{pmatrix}, \tag{3}$$

where $\hbar\omega_{7,8}=2\hbar^2k_0^2(1\mp\cos\vartheta)/m^*$. We calculate the effective coupling V_{D} as the Hamiltonian matrix element $\langle\Psi_{\mathrm{f}}|H'|\Psi_{\mathrm{i}}\rangle$, where $\Psi_{\mathrm{i,f}}$ are the initial and the final states, respectively, and H' is the microscopic diffraction Hamiltonian relevant for the selected group of states. Let us take for instance the transition $E\rightarrow H$. In this case, the part of microscopic Hamiltonian which applies is $H'=V(a_7^+a_2^+a_3a_1+\mathrm{H.c.})$ and the initial and final states are

$$\Psi_{\mathrm{i}}=a_3^+a_4^+|n_1,n_2\rangle, \tag{4}$$

$$\Psi_{\mathrm{f}}=a_7^+a_4^+|n_1-1,n_2+1\rangle, \tag{5}$$

where $|n_1,n_2\rangle$ is a state created by pump beams with mean numbers of polaritons $n_{1,2}$ in the states 1 and 2, respectively. Considering $n_{1,2}\gg 1$, we finally obtain $V_{\mathrm{D}}=V\sqrt{n_1n_2}$.

Coupling of the states, according to the above Hamiltonians, is depicted in Fig. 1(c) by vertical lines. As we stated before, the two groups of states shown in this figure are coupled by EC scattering (whose amplitude is V). Note that not only the states A and E are coupled, we must take into

account also EC coupling of the virtual states. The coupled states are connected by horizontal lines in Fig. 1(c). The corresponding EC coupling Hamiltonian is

$$H_{\mathrm{EC}} = V[(|A\rangle + |D\rangle)(\langle E| + \langle J| + \langle K|) + |B\rangle(\langle F| + \langle H|) + |C\rangle(\langle G| + \langle I|) + \mathrm{H.c.}]. \quad (6)$$

Population of the polaritons scattered to a fixed angle ϑ is defined by $N_{\mathrm{tot}}(\vartheta)=2\Sigma_{\ell=E}^{K} n_\ell(\vartheta)$, where n_ℓ are the individual populations of the states $E-K$ and the prefactor "2" arises due to the two-particle nature of the states. This definition includes both contributions from the EC states and diffracted polaritons lying on the off-branches. To account only for the states on the EC, the definition should be revised

$$N_{\mathrm{EC}}(\vartheta) = 2n_E + \sum_{\ell=F}^{I} n_\ell. \quad (7)$$

We evaluate the population $N_{\mathrm{EC}}(\vartheta)$ within the second-order perturbation theory for the EC scattering. On the other hand, we account for the diffraction by exact diagonalization of the appropriate Hamiltonians due to the large coupling terms. All states are then divided to the groups, whose kinetics is treated nonperturbatively while the intergroup interactions are expanded to perturbation series. It is then straightforward to diagonalize the particular group Hamiltonians: $H_{a-d}=T^{(0)}H_{A-D}T^{(0)^+}$ and $H_{e-k}=T^{(\vartheta)}H_{E-K}T^{(\vartheta)^+}$, where $T^{(m)}$ are the relevant transformation matrices. By this diagonalization, we define a new set of eigenenergies $\hbar\omega_a,\ldots,\hbar\omega_k$, eigenstates $|a\rangle=\Sigma_{\ell=A}^{D}T_{a,\ell}^{(0)}|\ell\rangle$ etc. as a linear combination of the original states. The EC populations may be then redefined as $N_{\mathrm{EC}}(\vartheta)=\Sigma_{\ell=e}^{k} n_\ell(\vartheta)P_\ell(\vartheta)$, factor $P_\ell(\vartheta)$ being a number of the polaritons from the state $|\ell\rangle$ lying on the EC [cf. Eq. (7)],

$$P_\ell(\vartheta) = 2[T_{\ell,E}^{(\vartheta)}]^2 + \sum_{j=F}^{I} [T_{\ell,j}^{(\vartheta)}]^2. \quad (8)$$

Applying the standard second-order perturbative approach, we obtain the steady-state population of, e.g., a final state f in the form

$$n_f = \frac{2}{\hbar^2}\sum_{\ell=a}^{d} \frac{|(H_{\mathrm{EC}})_{f,\ell}|^2}{\Gamma^2 + (\omega_f - \omega_\ell)^2} n_\ell, \quad (9)$$

where Γ is the polariton dephasing rate. Considering further the initial condition $n_A=n_1=n_2$, and $n_{B-D}=0$, we obtain after transformation $n_{a-d}=|T_{a-d,A}^{(0)}|^2 n_A$ and the EC scattering Hamiltonian is transformed as $(H_{\mathrm{ec}})_{\ell,j}=\Sigma_{m,n}T_{\ell,m}^{(\vartheta)}(H_{\mathrm{EC}})_{m,n}T_{j,n}^{(0)}$ (the last term comes from the Hermitian conjugate of a real matrix). Substituting this expression to the above equation and considering explicit form (6) of the EC scattering Hamiltonian, we finally obtain

$$N_{\mathrm{EC}}(\vartheta) = \frac{V^2 n_1}{\hbar^2}\sum_{j=a}^{d}\sum_{\ell=e}^{k} \frac{[T_{j,A}^{(0)}]^2 P_\ell(\vartheta)}{(\omega_j - \omega_\ell)^2 + \Gamma^2} \sum_{[m,n]} |T_{j,m}^{(0)} T_{\ell,n}^{(\vartheta)}|^2, \quad (10)$$

$$[m,n] \in \{[A,E];[A,J];[A,K];[B,F];[B,H];[C,G];[C,I];[D,E];[D,J];[D,K]\}. \quad (11)$$

The above equation is the illustrative result considering only one circular polarization and resonant scattering on the EC. In reality, however, one usually deals with both polarizations and the polariton population distributed in the whole reciprocal space. To account for all possible final states, we simply let the state E be anywhere in the reciprocal space and directly apply the equations above. Considering the spin, each polariton may carry an angular momentum ± 1 and therefore we redefine polariton states as, e.g., $|A\pm\pm\rangle=(1\pm,2\pm)$. Each of the two-polariton states A to K is then split to four levels having different spin configurations of the participating polaritons. Coupling strengths between the states are no more equal but depend on the spin configuration of the initial and final states and the spin-dependent populations of the initial states $n_{1\pm}$ and $n_{2\pm}$.

In the numerical calculation we take the polariton effective mass of $m^*=10^{-5}m_{\mathrm{e}}$, where m_{e} is a free-electron mass, the in-plane momentum of the pump beams $k_0=0.9\ \mu\mathrm{m}^{-1}$ and the dephasing rate $\Gamma=0.2\ \mathrm{ps}^{-1}$. We calculated the distributions of polariton populations in the k-space, using the second-order perturbation theory without stimulation of the EC scattering, keeping scattering amplitudes $V_{1,2}$ (scattering of polaritons with parallel or antiparallel spins, respectively[18]) constant around the EC and considering various combinations of polarizations of the excitation beams. The result for cocircular polarizations is shown in Fig. 2(a). Clearly the polariton population is distributed in the vicinity of the EC with the radius $0.9\ \mu\mathrm{m}^{-1}$ and is further modulated depending on the scattering angle. Note, however, that this modulation is due to the coupling to the virtual states by diffraction on the pump-induced grating. The evaluated polariton population $N(k=k_0,\vartheta)$ on the EC is depicted in Fig. 2(b), and Fig. 2(c) shows its wave-vector dependence for three fixed values of the scattering angle.

It follows from Fig. 2(b) that the polariton population depends on the spins of interacting polaritons and the spin structure of the excitation beams. Scattering of cocircularly or linearly polarized beams demonstrates preferential spontaneous scattering to the angles around 90°, while counter-circularly polarized beams are preferentially backscattered. According to Fig. 2(c), diffraction also causes variations of the radial distribution of the polariton density around the EC.

In the case of the linear copolarized excitation beams the scattering is accompanied by inversion of the linear polarization, as it was noticed in Refs. 8, 16, and 18. The inversion of polarization results from the interplay of first-order

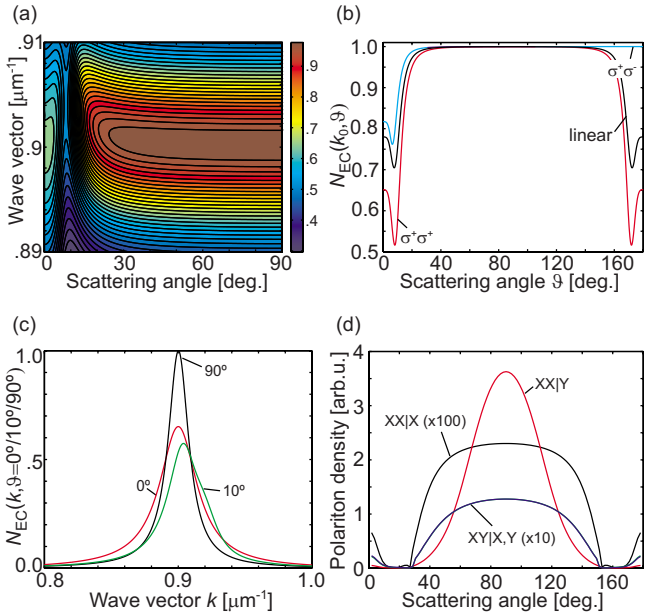

FIG. 2. (Color online) (a) Calculated steady-state populations of the polariton states in the k space for the cocircular polarizations of excitation beams (far below stimulation threshold). (b) Population of the EC for various combinations of the polarizations of the pump beams. (c) Population of the polariton states at scattering angles 0, 10, and 90° for cocircularly polarized excitation. (d) Polarization-resolved steady-state polariton population on the EC under strong cw excitation slightly above threshold (1.12 P_{thr}) with colinear or crosslinear polarizations. Notation $AB|C$ means that excitation beams have polarizations A and B, and C-polarized component is detected ($A,B,C=X,Y$).

polariton-polariton exchange interaction between the copolarized components in the circular spin basis and the second-order exchange process between countercircularly polarized components via dark states.[22] The second-order exchange process is comparable in magnitude to the first-order exchange process, due to the high density of intermediate dark states characterized by the excitonlike dispersion. The polarization degree of the scattered states may be estimated from the T matrix for polariton-polariton interaction.[23] Note, however, that the calculation of Schumacher *et al.* comprises a two-dimensional approximation of the exciton gas and therefore the use of the T matrix itself may result in an overestimation of the polarization degree because of the neglect of the direct-scattering channel.[18] Using the algebra of Ref. 18 and considering $T_{\mathrm{R}}^{+-}/T_{\mathrm{R}}^{++}=-0.28$ from Ref. 23, we find for the degree of linear polarization

$$\rho_{\ell}=\frac{2T_{\mathrm{R}}^{+-}/T_{\mathrm{R}}^{++}}{1+(T_{\mathrm{R}}^{+-}/T_{\mathrm{R}}^{++})^2}\approx -52\%. \tag{12}$$

The negative sign here means that the polarization plane of the final states is rotated by 90° with respect to the polarization of the pump beams. Compared to the experimental data of Ref. 6, the polarization degree we obtain is 2.5 times higher. In the real experiment, the final linear polarization degree could have been reduced due to the self-induced Larmor precession of polariton pseudospins, neglected in our model. If the pumps are linearly crosspolarized the scattering results in a depolarized signal around the EC as discussed in Ref. 18 while only a small polarization degree resulting from the weak direct-scattering term is expected.

Preferential scattering to the 90° direction shown in Fig. 2(a) may be qualitatively explained in terms of the above simplified model with levels $A-K$ ascribed to one circular polarization. As noted in the beginning of this section, polaritons may remain in the virtual state for a limited time inversely proportional to the virtual state detuning from the EC. Clearly the larger time polaritons are in the virtual state, the larger influence of the diffraction is and the larger (negative) modulation of the coupling strength is. Scattering is therefore the least influenced by diffraction if the virtual states are separated from the EC by the largest amount of energy, what is actually the case of scattering to the angle $\vartheta=90°$. If $\vartheta\approx 0$ or 180°, on the contrary, small energy separation of the levels F,G or H,I from the level E causes relatively high population of the virtual off-branch states and therefore large reduction of the coupling strength between the initial state and the states on the elastic circle.

III. POLARITON X-NOR GATE IN THE STIMULATED REGIME

The above discussion of the regime of spontaneous scattering proves our assumption that the excitation causes the symmetry breaking resulting in the modulation of the polariton-polariton scattering amplitudes. In the spontaneous regime this modulation is rather weak and hardly can be experimentally detected. However, the effect can be drastically amplified in the stimulated regime. Stimulation provides also the dramatic increase of linear polarization degree of the scattered beams which may achieve almost 100%.

For the analysis of the stimulated scattering case we shall operate with the spin-density matrix of the system using the first-order Born-Markov approximation. Consider the particles which can scatter from initial states 1 and 2 to final states 3 and 4 on the EC. The appropriate part of the interaction Hamiltonian can be written as $H_{\mathrm{scatt}}=H^{+}+H^{-}$ where

$$\begin{aligned}H^{+}=&V_1(a_{1+}^{+}a_{2+}^{+}a_{3+}a_{4+}+a_{1-}^{+}a_{2-}^{+}a_{3-}a_{4-})\\&+V_2(a_{1+}^{+}a_{2-}^{+}a_{3+}a_{4-}+a_{1-}^{+}a_{2+}^{+}a_{3-}a_{4+})\\&+V_3(a_{1+}^{+}a_{2-}^{+}a_{3-}a_{4+}+a_{1-}^{+}a_{2+}^{+}a_{3+}a_{4-}),\end{aligned} \tag{13}$$

and $H^{-}=(H^{+})^{+}$. Scattering amplitudes are denoted V_{1-3} here, V_1 describing the spin triplet configuration and $V_{2,3}$ describing the singlet configuration. In order to account for the diffraction on the transient grating, we do not further introduce the virtual states in the Hamiltonian but rather consider V_{1-3} as effective scattering amplitudes defined as

$$V_j(\vartheta)=\frac{N_{\mathrm{EC}}(\vartheta)}{N'_{\mathrm{EC}}(\vartheta)}\tilde{V}_j(\vartheta), \tag{14}$$

where $N(\vartheta)$ and $N'(\vartheta)$ come from Eq. (10) as the populations coupled and uncoupled to the virtual states, respectively. The decoupling of the EC scattering and the diffraction present in the Eq. (14) is valid as long as we may

consider that diffraction on the grating formed by pump beams is the strongest process in the system. We therefore require $n_{1,2} \gg n_{3,4}$ otherwise the large population of the states on EC would introduce a new efficient diffraction channel and the approximation of Eq. (14) would break. The condition is satisfied in the experiment of Ref. 16. The bare scattering amplitude $\tilde{V}_j(\vartheta)$ can be estimated using microscopic calculations,[22,24] considering the amplitude of the direct scattering in real three-dimensional structures.[18] The second-order exchange processes do not contribute to the Hamiltonian in the basis restricted to the bright states only, however the Hamiltonian presented above may be regarded as an effective one with the scattering amplitudes which give a correct form of the scattering T matrix within the chosen Born-Markov approximation. The second-order processes therefore may be accounted for in the scattering amplitudes $V_{2,3}$.

The Liouville–von Neumann equation for the density matrix ϱ of the system reads as ($\hbar=1$)

$$\partial_t \varrho = -\int_{-\infty}^{t} \{H_{\text{scatt}}(t);[H_{\text{scatt}}(t');\varrho(t')]\}. \tag{15}$$

In the Born-Markov approximation one replaces t' by t and retains only energy-conserving terms which yields

$$\delta^{-1}(\Delta E)\partial_t \varrho = 2(H^+\varrho H^- + H^-\varrho H^+) - (H^+H^- + H^-H^+)\varrho - \varrho(H^+H^- + H^-H^+) \tag{16}$$

where the term $\delta^{-1}(\Delta E)$ ensures the conservation of energy. For time evolution of the mean values of any arbitrary operator $\hat{A}$, $\langle\hat{A}\rangle = \mathrm{Tr}(\varrho\hat{A})$ one has

$$\partial_t\langle\hat{A}\rangle = \mathrm{Tr}(\varrho[H^-;[\hat{A};H^+]]) + \mathrm{Tr}(\varrho[H^+;[\hat{A};H^-]]). \tag{17}$$

This formula can be used for calculation of temporal dynamics of the occupancies and pseudospins defined as

$$N_j = \mathrm{Tr}\{\varrho(a^+_{j,+}a_{j,+} + a^+_{j,-}a_{j,-})\}, \tag{18}$$

$$S_{x,j} = \mathrm{Re}\ \mathrm{Tr}\{\varrho a^+_{j,+}a_{j,-}\}, \tag{19}$$

$$S_{y,j} = \mathrm{Im}\ \mathrm{Tr}\{\varrho a^+_{j,+}a_{j,-}\}, \tag{20}$$

$$S_{z,j} = \frac{1}{2}\mathrm{Tr}\{\varrho(a^+_{j,+}a_{j,+} - a^+_{j,-}a_{j,-})\}. \tag{21}$$

The resulting explicit formulas are listed in the Appendix. Figure 2(d) shows the resulting distributions of polaritons on the EC in the stimulated regime under different excitation conditions (the pump beams are subtracted). One can see that the colinear excitation exceeds 98.5% spin inversion slightly above the threshold (the spin inversion further increases with increasing pump power) and a strong emission in the 90° direction with full width at half maximum of 50°, in accordance with the experimental data of Ref. 16. Crosslinear excitation, on the other hand, for the same excitation intensity yields the scattering signal which is more that one order of magnitude weaker and is almost unpolarized.

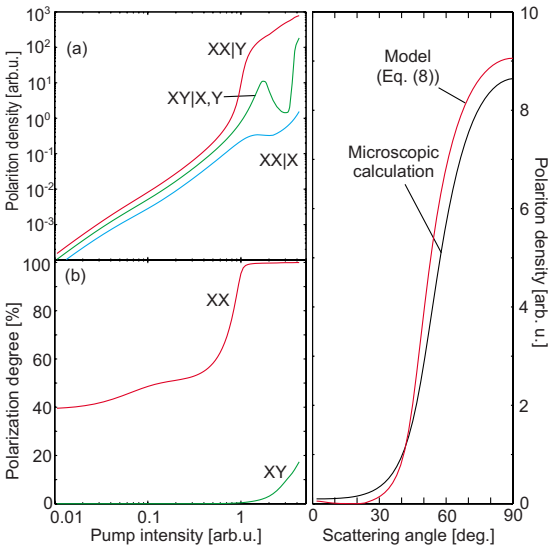

FIG. 3. (Color online) (a) Pump intensity dependence of the polarized polariton population on the EC. The polariton population at the scattering angle 90° under different pump and detection conditions is shown. Pump intensity is plotted relative to the threshold for the colinear excitation. (b) Pump intensity dependence of the maximum of polarization degree for colinearly (red) and crosslinearly (green) polarized pumps. The sign of the polarization degree shown by the red curve is inverted for clarity. (c) Comparison of the full microscopic calculation and the presented model for pump power of 1.12 units, assuming cocircular polarizations of the excitation beams.

In order to explain why the polariton-polariton scattering and polarization inversion under colinear pump is stronger by orders of magnitude than the scattering with crosslinearly polarized beams, we plot the intensity dependence of the polariton population and the maximum polarization degree in Figs. 3(a) and 3(b). The gate performance in Fig. 2(d) is plotted for the pump intensity of 1.12 (in the units corresponding to the horizontal scale in Fig. 3). The stimulation threshold is reached for the colinear but not crosslinear pumps, which is why the scattered signal is so much different in the two cases. The gate may therefore operate only within the interval of pump intensities between the two stimulation thresholds for colinear and crosslinear pump polarizations.

The initial degree of polarization at very low pump power is about −40% in the present calculation, which is far below the experimentally observed value[6] −(15–20)% and also below our theoretical prediction −11% for the narrow InGaAs QWs.[18] There is no contradiction with our previous publication[18] as here we consider an 8-nm-wide QW while the QW of 2.5 nm width has been considered in Ref. 18. As the QW width determines the magnitude of the direct-scattering term, the linear polarization degree of the scattered polaritons in an 8-nm-wide QW is much higher compared to a 2.5-nm-wide QW. Considering further complex polarization dynamics in the case of the excitation geometry of Ref. 6, we find that the theoretical estimation and experimental data are fully compatible.

Figure 3(b) illustrates another interesting feature of the stimulated scattering on the EC. Although the polarization

degree in the spontaneous regime of scattering of crosslinearly polarized polaritons does not exceed 0.1%, stimulation causes the polarization amplification, which is essential for operation of future spin-optronic devices.

The use of approximation (14) simplifies the calculations significantly and also allows one to understand the physical origin of the population modulation on the EC observed in experiments. We verified the accuracy of Eq. (14) by a numerical calculation. For this purpose, we have derived the kinetic equations for the polariton system on the elastic circle in the stimulation regime accounting for the diffraction in the microscopic Hamiltonian and thus without simplifying assumption of Eq. (14). We have used the same approach as in Sec. II; i.e., we have considered the same states involved in the dynamics, the diffraction (restricted to the first diffraction maxima only) has been accounted for nonperturbatively and the EC scattering has been considered within the Born-Markov approximation. Considering cocircular excitation for simplicity, we obtain in this way the results depicted in Fig. 3(c) using the same input parameters for the exact and simplified calculations. One can see that even though there is some small difference between the curves, the approximate model still gives very good predictions.

IV. CONCLUSIONS

We have analyzed the most efficient channels of polariton-polariton scattering on the elastic circle in terms of multiwave mixing. We show that the multiple polariton scattering processes are responsible for changes in the scattering probability of the order of few percents in the linear regime. The increase in the excitation intensity leads to a drastic increase in this modulation due to the final-state bosonic stimulation. The multiple polariton scattering process can be conveniently represented as a combination of the polariton scattering with a subsequent diffraction to the off-branch states by a polarization grating created by two pump pulses. The polaritons from off-branch states then go back to the elastic circle, so that the energy is conserved.

This scenario explains preferential scattering of the polaritons at 90° in the case of colinearly polarized light beams. In this case, none of the intermediate off-branch states is close in energy to the elastic circle polaritons so that destructive interference caused by virtual diffraction processes is suppressed.

We show that the polarization degree of the scattered polaritons strongly depends on the pump intensity and that the final polarization degree may be strongly amplified above the stimulation threshold. This feature opens a possibility of construction of a spin-optronic transistor with a smooth dependence of the output polarization on the polarization of the gate input. The results of this work may be applied for optimization of the design of polariton logic gates by considering various spin configurations or introducing more control beams.

ACKNOWLEDGMENTS

We thank Y. G. Rubo for enlightening discussions. T.O. and A.V.K. acknowledge support from EPSRC-GB and the Chair of Excellence grant POLAROMA.

APPENDIX

We define the scattering probabilities as $W_j=|V_j|^2$ and $W_{j\ell}=V_jV_\ell^*=W_{12}^{\mathrm{R}}+\mathrm{i}W_{12}^{\mathrm{I}}$. Following Eq. (17) and definitions (18)–(21), we obtain the following equations of motion for the different pseudospin components. Polariton population

$$\frac{d}{dt}N_3 = N_{11} + N_{12} + N_{22} + N_{13} + N_{23} + N_{33},$$

$$N_{11} = \frac{W_1}{2}[(N_1N_2 + 4S_{1z}S_{2z})(N_3 + N_4 + 2) - (N_3N_4 + 4S_{3z}S_{4z})(N_1 + N_2 + 2)]$$
$$+ 2W_1[(N_1S_{2z} + S_{1z}N_2)(S_{3z} + S_{4z}) - (S_{1z} + S_{2z})(S_{3z}N_4 + N_3S_{4z})],$$

$$N_{12} = 4W_{12}^R[(N_1 - N_3)\boldsymbol{S}_2 \cdot \boldsymbol{S}_4 + (N_2 - N_4)\boldsymbol{S}_1 \cdot \boldsymbol{S}_3] + 8W_{12}^I[(S_{1z} - S_{3z})\boldsymbol{S}_2 \times \boldsymbol{S}_4 + (S_{2z} - S_{4z})\boldsymbol{S}_1 \times \boldsymbol{S}_3],$$

$$N_{22} = \frac{W_2}{2}[(N_1N_2 - 4S_{1z}S_{2z})(N_3 + N_4 + 2) - (N_3N_4 - 4S_{3z}S_{4z})(N_1 + N_2 + 2)]$$
$$- 2W_2[(N_1S_{2z} - S_{1z}N_2)(S_{3z} - S_{4z}) - (S_{1z} - S_{2z})(N_3S_{4z} - S_{3z}N_4)],$$

$$N_{13} = 4W_{13}^R[(N_1 - N_4)\boldsymbol{S}_2 \cdot \boldsymbol{S}_3 + (N_2 - N_3)\boldsymbol{S}_1 \cdot \boldsymbol{S}_4] + 8W_{13}^I[(S_{1z} - S_{4z})\boldsymbol{S}_2 \times \boldsymbol{S}_3 + (S_{2z} - S_{3z})\boldsymbol{S}_1 \times \boldsymbol{S}_4],$$

$$N_{23} = -4W_{23}^R[(N_1 + N_2 + 2)\boldsymbol{S}_3 \cdot \boldsymbol{S}_4 - (N_3 + N_4 + 2)\boldsymbol{S}_1 \cdot \boldsymbol{S}_2] + 8W_{23}^I[(S_{1z} - S_{2z})\boldsymbol{S}_3 \times \boldsymbol{S}_4 + (S_{3z} - S_{4z})\boldsymbol{S}_1 \times \boldsymbol{S}_2],$$

$$N_{33} = \frac{W_3}{2}[(N_1N_2 - 4S_{1z}S_{2z})(N_3 + N_4 + 2) - (N_3N_4 - 4S_{3z}S_{4z})(N_1 + N_2 + 2)]$$

$$- + 2W_3[(N_1S_{2z} - S_{1z}N_2)(S_{3z} - S_{4z}) - (S_{1z} - S_{2z})(N_3S_{4z} - S_{3z}N_4)].$$

Z component of the pseudospin

$$\frac{d}{dt}S_{3z} = Z_{11} + Z_{12} + Z_{22} + Z_{13} + Z_{23} + Z_{33},$$

$$Z_{11} = \frac{W_1}{2}[(N_1S_{2z} + S_{1z}N_2)(N_3 + N_4 + 2) - (N_1 + N_2 + 2)(N_3S_{4z} + S_{3z}N_4)]$$

$$+ \frac{W_1}{2}[(N_1N_2 + 4S_{1z}S_{2z})(S_{3z} + S_{4z}) - (S_{1z} + S_{2z})(N_3N_4 + 4S_{3z}S_{4z})],$$

$$Z_{12} = 4W_{12}^R(S_{1z} - S_{3z})\boldsymbol{S}_2 \cdot \boldsymbol{S}_4 + 2W_{12}^I(N_1 - N_3)\boldsymbol{S}_2 \times \boldsymbol{S}_4,$$

$$Z_{22} = -\frac{W_2}{2}[(N_1S_{2z} - S_{1z}N_2)(N_3 + N_4 + 2) - (N_1 + N_2 + 2)(N_3S_{4z} - S_{3z}N_4)]$$

$$+ \frac{W_2}{2}[(N_1N_2 - 4S_{1z}S_{2z})(S_{3z} - S_{4z}) - (S_{1z} - S_{2z})(N_3N_4 - 4S_{3z}S_{4z})],$$

$$Z_{13} = 4W_{13}^R(S_{2z} - S_{3z})\boldsymbol{S}_1 \cdot \boldsymbol{S}_4 + 2W_{13}^I(N_2 - N_3)\boldsymbol{S}_1 \times \boldsymbol{S}_4,$$

$$Z_{23} = 4W_{23}^R(S_{3z} - S_{4z})\boldsymbol{S}_1 \cdot \boldsymbol{S}_2 + 2W_{23}^I(N_3 + N_4 + 2)\boldsymbol{S}_1 \times \boldsymbol{S}_2,$$

$$Z_{33} = \frac{W_3}{2}[(N_1S_{2z} - S_{1z}N_2)(N_3 + N_4 + 2) + (N_1 + N_2 + 2)(N_3S_{4z} - S_{3z}N_4)]$$

$$+ \frac{W_3}{2}[(N_1N_2 - 4S_{1z}S_{2z})(S_{3z} - S_{4z}) + (S_{1z} - S_{2z})(N_3N_4 - 4S_{3z}S_{4z})].$$

Y component of the pseudospin

$$\frac{d}{dt}S_{3y} = Y_{11} + Y_{12} + Y_{22} + Y_{13} + Y_{23} + Y_{33}$$

$$Y_{11} = -\frac{W_1}{2}[N_4(N_1 + N_2 + 2) - N_1N_2]S_{3y} - 2W_1[S_{4z}(S_{1z} + S_{2z}) - S_{1z}S_{2z}]S_{3y} + 2W_1[S_{2y}\boldsymbol{S}_1 \cdot \boldsymbol{S}_4 - S_{2x}\boldsymbol{S}_1 \times \boldsymbol{S}_4],$$

$$Y_{12} = W_{12}^R[N_2(N_3 + N_4 + 2) - N_3N_4 + 4S_{2z}S_{4z}]S_{1y} - 4W_{12}^RS_{3y}\boldsymbol{S}_2 \cdot \boldsymbol{S}_4 + 2W_{12}^I[S_{2z}(N_3 + N_4 + 2) + S_{4z}(N_2 - N_3)]S_{1x},$$

$$Y_{22} = -\frac{W_2}{2}[N_4(N_1 + N_2 + 2) - N_1N_2]S_{3y} + 2W_2[S_{4z}(S_{1z} - S_{2z}) - S_{1z}S_{2z}]S_{3y} + 2W_2[S_{1y}\boldsymbol{S}_2 \cdot \boldsymbol{S}_4 + S_{1x}\boldsymbol{S}_2 \times \boldsymbol{S}_4],$$

$$Y_{13} = W_{13}^R[N_1(N_3 + N_4 + 2) - N_3N_4 + 4S_{1z}S_{4z}]S_{2y} - 4W_{13}^RS_{3y}\boldsymbol{S}_1 \cdot \boldsymbol{S}_4 + 2W_{13}^I[S_{1z}(N_3 + N_4 + 2) + S_{4z}(N_1 - N_3)]S_{2x},$$

$$Y_{23} = -W_{23}^R[N_3(N_1 + N_2 + 2) - N_1N_2 + 4S_{1z}S_{2z}]S_{4y} + 4W_{23}^RS_{3y}\boldsymbol{S}_1 \cdot \boldsymbol{S}_2 + 2W_{23}^I[S_{1z}(N_2 - N_3) - S_{2z}(N_1 - N_3)]S_{4x},$$

$$Y_{33} = -\frac{W_3}{2}[N_4(N_1 + N_2 + 2) - N_1N_2]S_{3y} - 2W_3[S_{4z}(S_{1z} - S_{2z}) + S_{1z}S_{2z}]S_{3y} + 2W_3[S_{2y}\boldsymbol{S}_1 \cdot \boldsymbol{S}_4 + S_{2x}\boldsymbol{S}_1 \times \boldsymbol{S}_4].$$

X component of the pseudospin

$$\frac{d}{dt}S_{3x} = X_{11} + X_{12} + X_{22} + X_{13} + X_{23} + X_{33}$$

$$X_{11} = -\frac{W_1}{2}[N_4(N_1+N_2+2)-N_1N_2]S_{3x} - 2W_1[S_{4z}(S_{1z}+S_{2z})-S_{1z}S_{2z}]S_{3x} + 2W_1[S_{2x}\boldsymbol{S}_1\cdot\boldsymbol{S}_4 + S_{2y}\boldsymbol{S}_1\times\boldsymbol{S}_4],$$

$$X_{12} = W_{12}^R[N_2(N_3+N_4+2)-N_3N_4+4S_{2z}S_{4z}]S_{1x} - 4W_{12}^R S_{3x}\boldsymbol{S}_2\cdot\boldsymbol{S}_4 - 2W_{12}^I[S_{2z}(N_3+N_4+2)+S_{4z}(N_2-N_3)]S_{1y},$$

$$X_{22} = -\frac{W_2}{2}[N_4(N_1+N_2+2)-N_1N_2]S_{3x} + 2W_2[S_{4z}(S_{1z}-S_{2z})-S_{1z}S_{2z}]S_{3x} + 2W_2[S_{1x}\boldsymbol{S}_2\cdot\boldsymbol{S}_4 - S_{1y}\boldsymbol{S}_2\times\boldsymbol{S}_4],$$

$$X_{13} = W_{13}^R[N_1(N_3+N_4+2)-N_3N_4+4S_{1z}S_{4z}]S_{2x} - 4W_{13}^R S_{3x}\boldsymbol{S}_1\cdot\boldsymbol{S}_4 - 2W_{13}^I[S_{1z}(N_3+N_4+2)+S_{4z}(N_1-N_3)]S_{2y},$$

$$X_{23} = -W_{23}^R[N_3(N_1+N_2+2)-N_1N_2+4S_{1z}S_{2z}]S_{4x} + 4W_{23}^R S_{3x}\boldsymbol{S}_1\cdot\boldsymbol{S}_2 - 2W_{23}^I[S_{1z}(N_2-N_3)-S_{2z}(N_1-N_3)]S_{4y},$$

$$X_{33} = -\frac{W_3}{2}[N_4(N_1+N_2+2)-N_1N_2]S_{3x} - 2W_3[S_{4z}(S_{1z}-S_{2z})+S_{1z}S_{2z}]S_{3x} + 2W_3[S_{2x}\boldsymbol{S}_1\cdot\boldsymbol{S}_4 - S_{2y}\boldsymbol{S}_1\times\boldsymbol{S}_4].$$

[1] See, e.g., G. Khitrova, H. M. Gibbs, F. Jahnke, M. Kira, and S. W. Koch, Rev. Mod. Phys. **71**, 1591 (1999).

[2] J. Kasprzak, M. Richard, S. Kundermann, A. Baas, P. Jeambrun, J. M. J. Keeling, F. M. Marchetti, M. H. Szymańska, R. André, J. L. Staehli, V. Savona, P. B. Littlewood, B. Deveaud, and Le Si Dang, Nature (London) **443**, 409 (2006).

[3] A. Amo, D. Sanvitto, F. P. Laussy, D. Ballarini, E. del Valle, M. D. Martin, A. Lemaître, J. Bloch, D. N. Krizhanovskii, M. S. Skolnick, C. Tejedor, and L. Viña, Nature (London) **457**, 291 (2009).

[4] Scattering between cavity polaritons and dark exciton states has been studied experimentally and theoretically in I. A. Shelykh, L. Vina, A. V. Kavokin, N. G. Galkin, G. Malpuech, and R. Andre, Solid State Commun. **135**, 1 (2005).

[5] K. V. Kavokin, I. A. Shelykh, A. V. Kavokin, G. Malpuech, and P. Bigenwald, Phys. Rev. Lett. **92**, 017401 (2004).

[6] P. Renucci, T. Amand, X. Marie, P. Senellart, J. Bloch, B. Sermage, and K. V. Kavokin, Phys. Rev. B **72**, 075317 (2005).

[7] M. Combescot and O. Betbeder-Matibet, Phys. Rev. B **74**, 125316 (2006).

[8] D. N. Krizhanovskii, D. Sanvitto, I. A. Shelykh, M. M. Glazov, G. Malpuech, D. D. Solnyshkov, A. Kavokin, S. Ceccarelli, M. S. Skolnick, and J. S. Roberts, Phys. Rev. B **73**, 073303 (2006).

[9] I. A. Shelykh, A. V. Kavokin, and G. Malpuech, Phys. Status Solidi B **242**, 2271 (2005).

[10] J. Kasprzak, R. Andre, L. S. Dang, I. A. Shelykh, A. V. Kavokin, Yu. G. Rubo, K. V. Kavokin, and G. Malpuech, Phys. Rev. B **75**, 045326 (2007).

[11] I. A. Shelykh, K. V. Kavokin, A. V. Kavokin, G. Malpuech, P. Bigenwald, H. Deng, G. Weihs, and Y. Yamamoto, Phys. Rev. B **70**, 035320 (2004).

[12] W. Langbein, I. A. Shelykh, D. Solnyshkov, G. Malpuech, Yu. Rubo, and A. Kavokin, Phys. Rev. B **75**, 075323 (2007).

[13] I. A. Shelykh, G. Pavlovic, D. D. Solnyshkov, and G. Malpuech, Phys. Rev. Lett. **102**, 046407 (2009).

[14] T. C. H. Liew, A. V. Kavokin, and I. A. Shelykh, Phys. Rev. Lett. **101**, 016402 (2008).

[15] R. Johne, N. A. Gippius, G. Pavlovic, D. D. Solnyshkov, I. A. Shelykh, and G. Malpuech, Phys. Rev. Lett. **100**, 240404 (2008).

[16] C. Leyder, T. C. H. Liew, A. V. Kavokin, I. A. Shelykh, M. Romanelli, J. Ph. Karr, E. Giacobino, and A. Bramati, Phys. Rev. Lett. **99**, 196402 (2007).

[17] M. Romanelli, C. Leyder, J. Ph. Karr, E. Giacobino, and A. Bramati, Phys. Rev. Lett. **98**, 106401 (2007).

[18] T. Ostatnický, D. Read, and A. V. Kavokin, Phys. Rev. B **80**, 115328 (2009).

[19] P. G. Savvidis, C. Ciuti, J. J. Baumberg, D. M. Whittaker, M. S. Skolnick, and J. S. Roberts, Phys. Rev. B **64**, 075311 (2001).

[20] The first-order approach in EC scattering is valid if the populations of the initial states exceed the remaining populations what is always fulfilled below the stimulation threshold. Second-order diffraction processes either restore the initial populations or populate states far away from the EC so that neglect of the states populated by the second-order diffraction processes is safe as well. The first-order approximation may fail, however, in the close vicinity to the excitation beams due to energy renormalizations and parametric interactions involving polaritons from one beam only. The criterion of validity of our approximation is $1-\cos\vartheta > Vm^*\sqrt{n_1 n_2}/2\hbar^2 k_0^2$ and results beyond this value may be significantly affected by the approximation. The estimates of the limiting angles in our calculations are $\vartheta > 6°$ in Figs. 2(a)–2(c) and $\vartheta > 12°$ in Figs. 2(d) and 3(c). The experiment shows a pronounced anisotropy of scattering for larger angles, with the maxima of scattering intensity around $\vartheta = 90°$. These states are perfectly within the limits of validity our model.

[21] D. D. Solnyshkov, I. A. Shelykh, N. A. Gippius, A. V. Kavokin, and G. Malpuech, Phys. Rev. B **77**, 045314 (2008).

[22] M. M. Glazov, H. Ouerdane, L. Pilozzi, G. Malpuech, A. V. Kavokin, and A. D'Andrea, Phys. Rev. B **80**, 155306 (2009).

[23] S. Schumacher, N. H. Kwong, and R. Binder, Phys. Rev. B **76**, 245324 (2007).

[24] M. Combescot, O. Betbeder-Matibet, and R. Combescot, Phys. Rev. B **75**, 174305 (2007).